

Supplementary Information

Molecular pathway and structural mechanism of human oncochannel TRPV6 inhibition by the phytocannabinoid tetrahydrocannabivarin

Arthur Neuberger¹, Yury A. Trofimov², Maria V. Yelshanskaya¹, Jeffrey Khau¹, Kirill D.
Nadezhdin¹, Lena S. Khosrof¹, Nikolay A. Krylov², Roman G. Efremov²,
Alexander I. Sobolevsky^{1,*}

¹ Department of Biochemistry and Molecular Biophysics, Columbia University, New York, NY,
USA

² Shemyakin-Ovchinnikov Institute of Bioorganic Chemistry, Russian Academy of Sciences,
Moscow, Russia

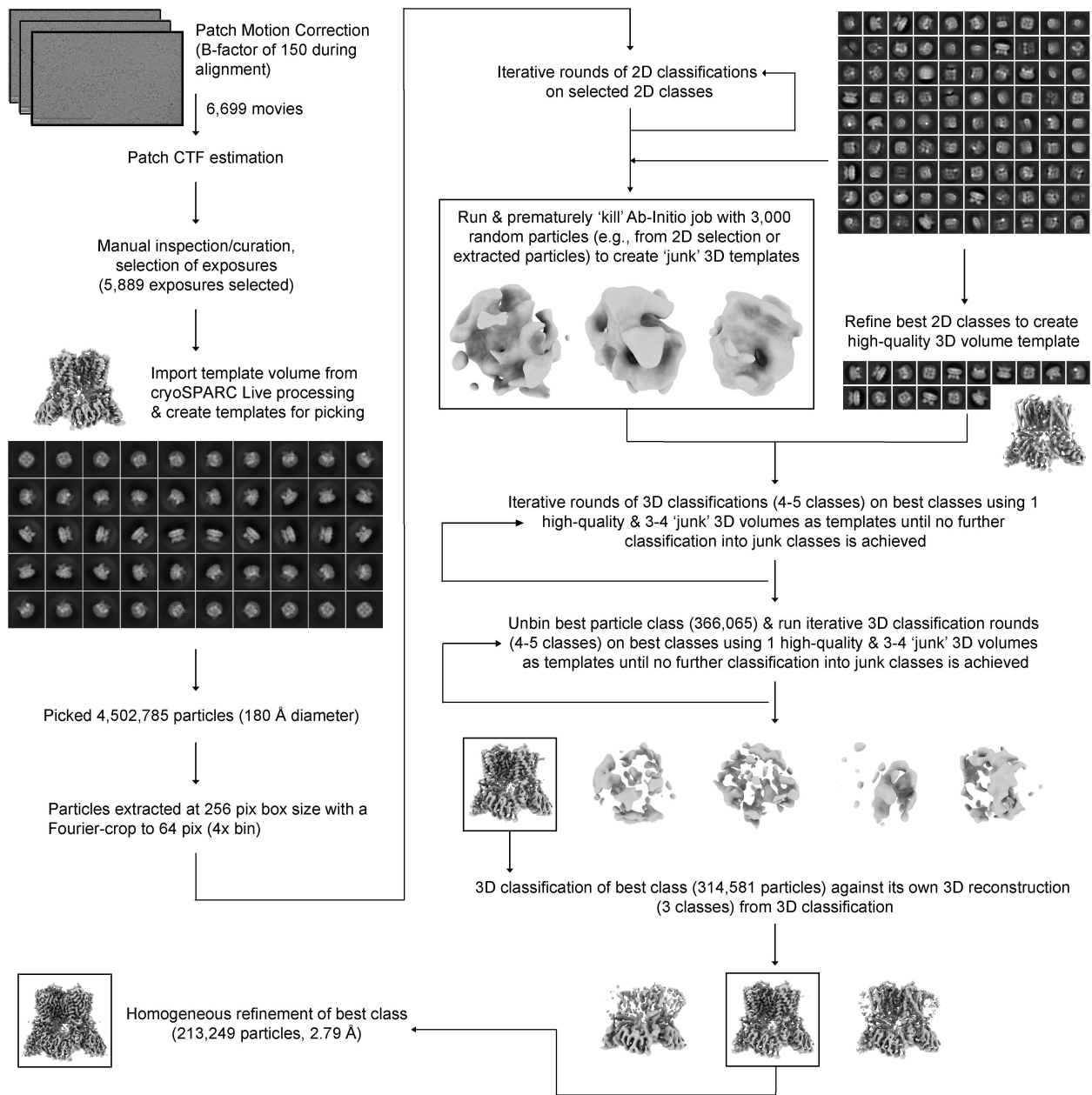
* Corresponding author. Tel: +1 2123054249; E-mail: as4005@cumc.columbia.edu

This PDF file includes:

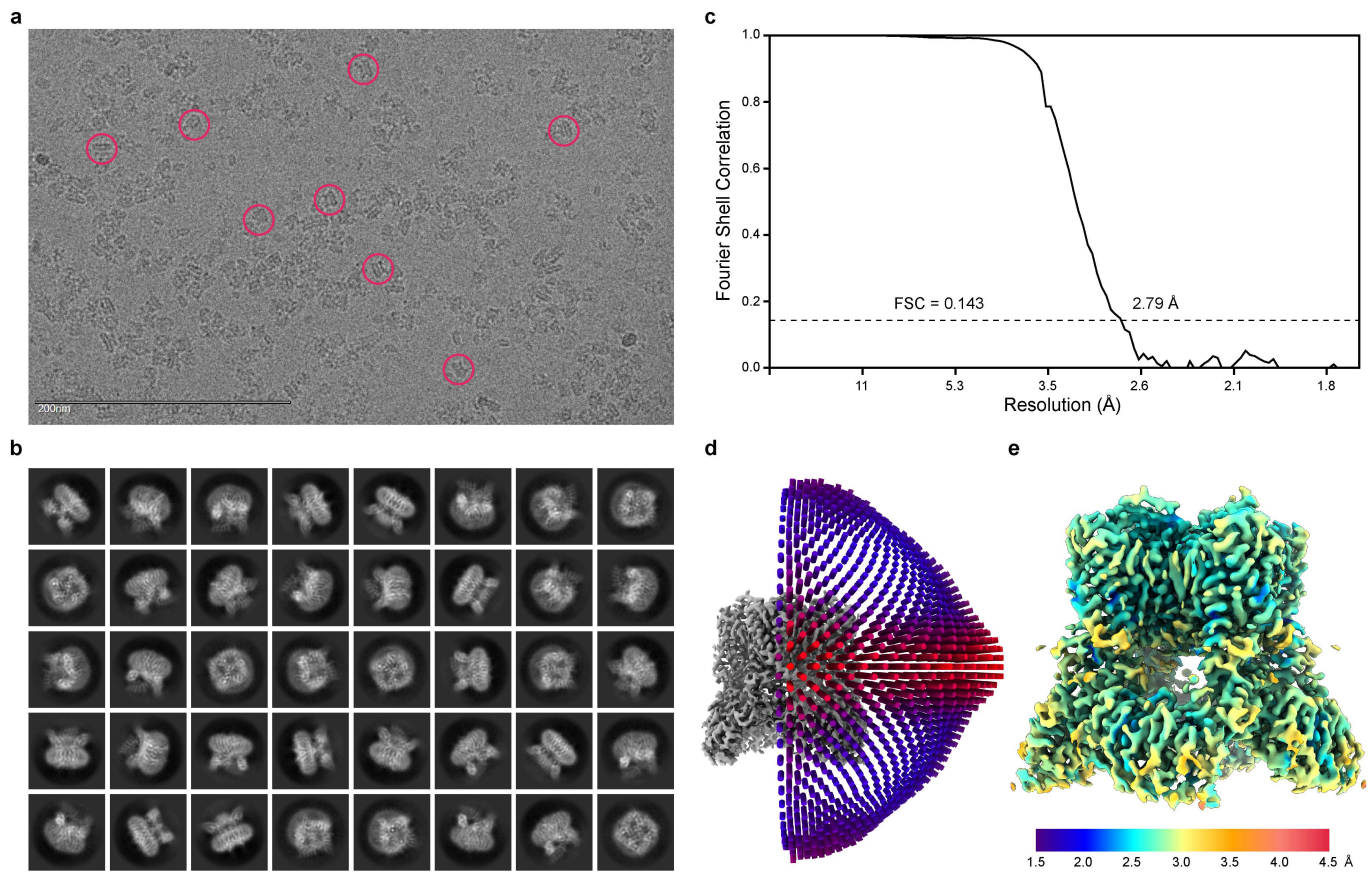
Supplementary Figures 1-8

Supplementary Table 1

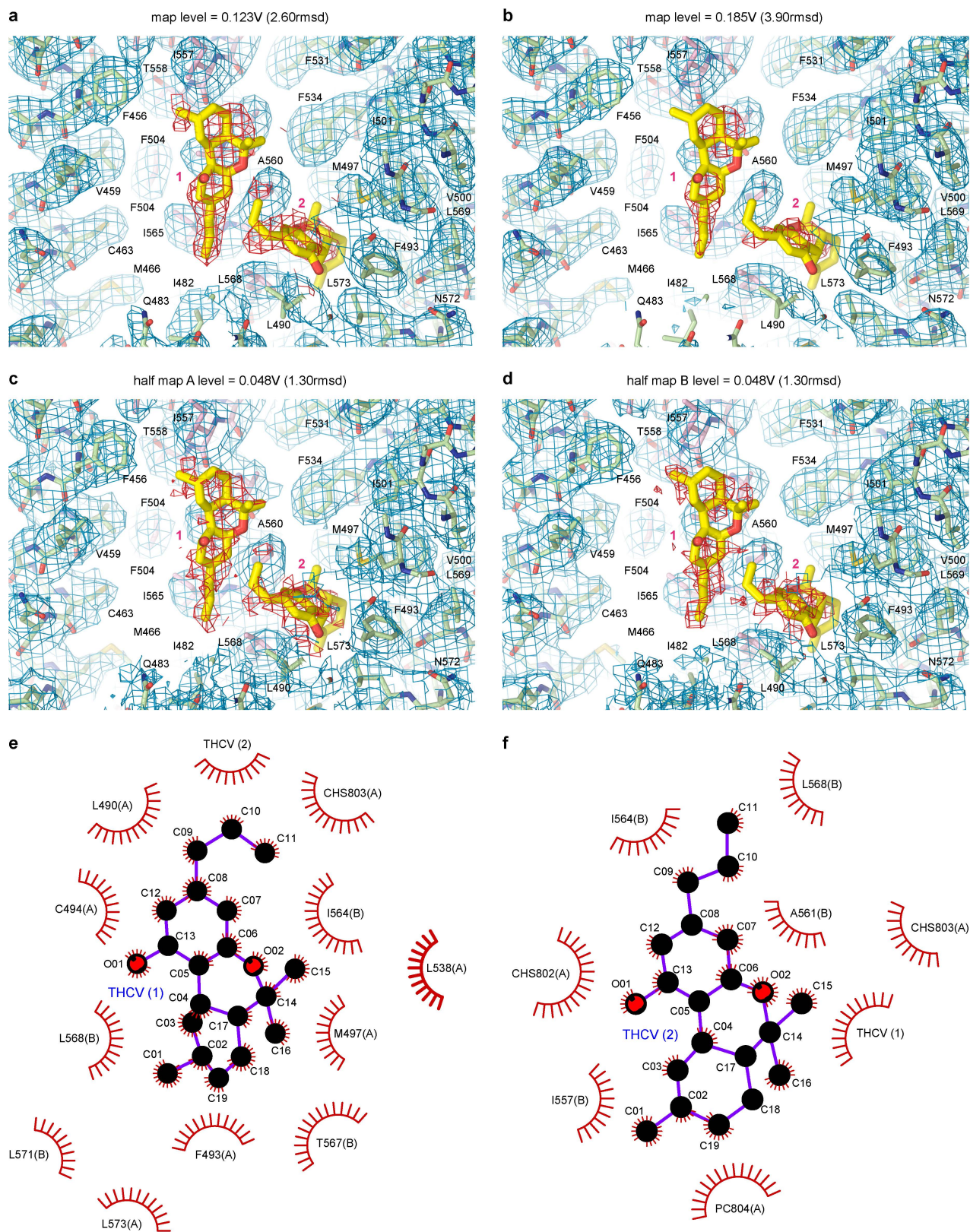
Supplementary References



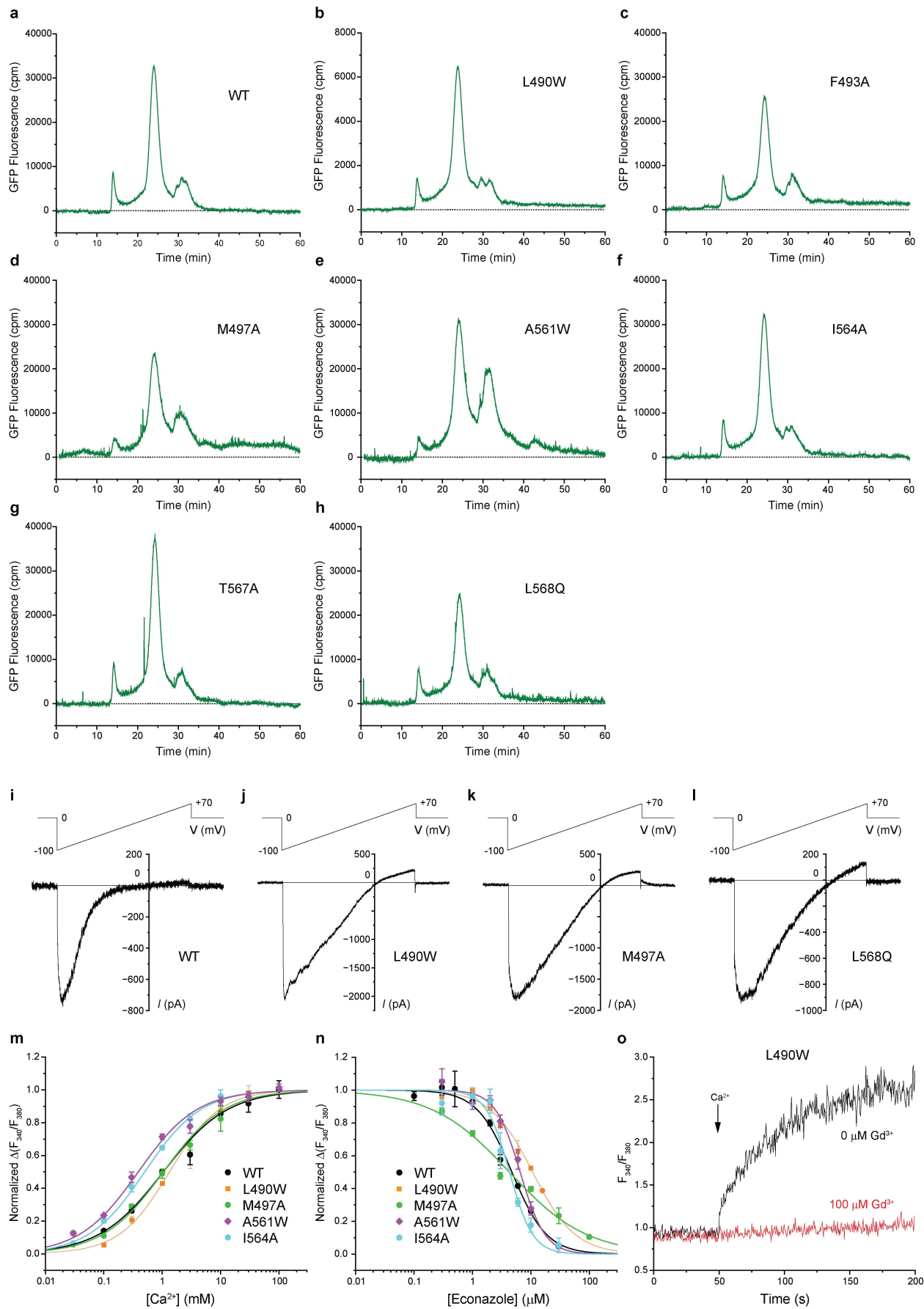
Supplementary Fig. 1 | 3D reconstruction workflow for hTRPV6_{THCV}. Examples of 2D class averages and 3D volumes are shown at different stages of cryo-EM data processing workflow.



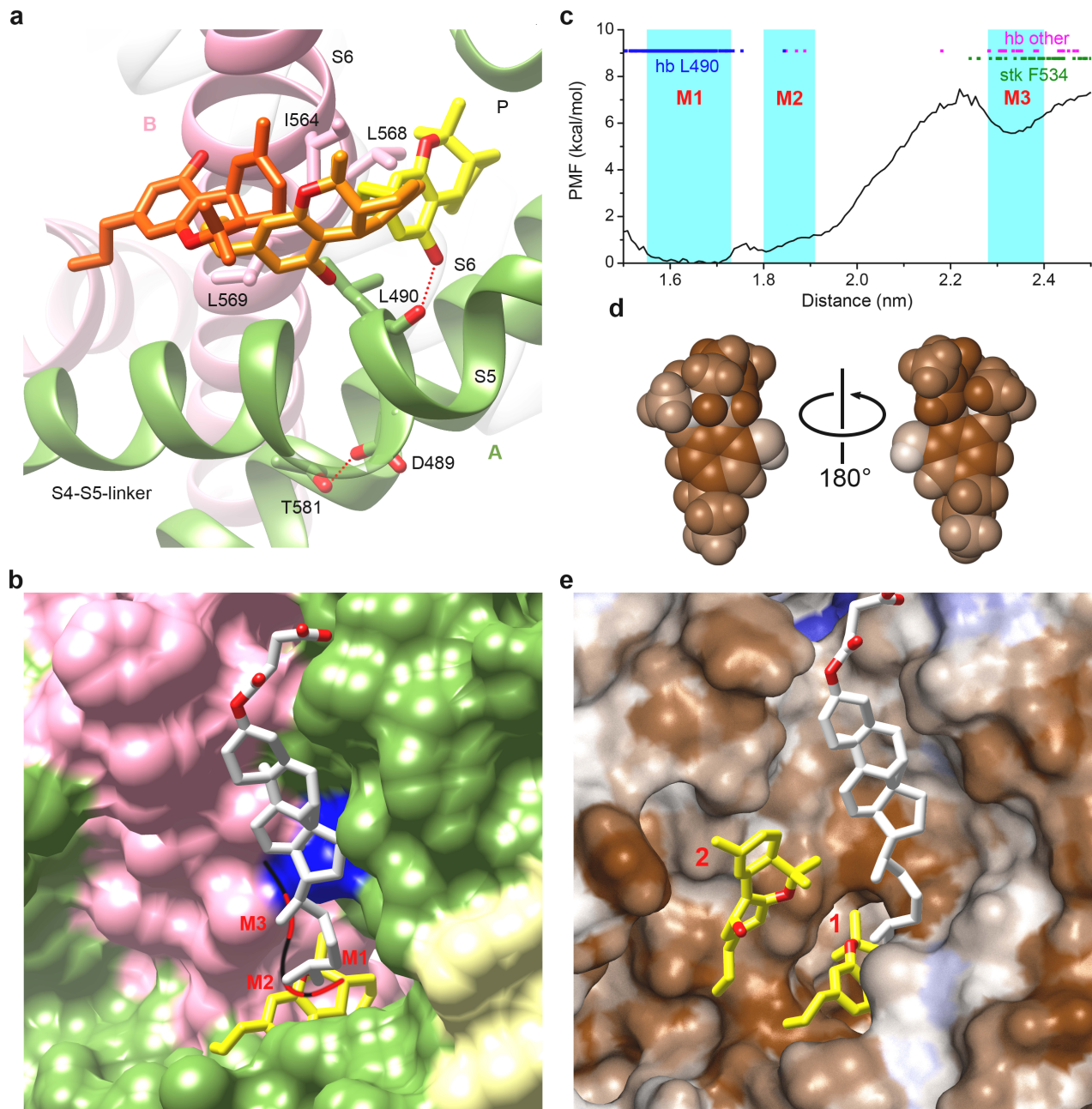
Supplementary Fig. 2 | Overview of cryo-EM data for hTRPV6_{THCV}. **a** Representative micrograph with example particles circled in pink. A total number of 6,699 such micrographs were collected. **b** Representative 2D class averages. **c** FSC curve. **d** Euler angle distribution of particles contributing to the final reconstruction with larger red cylinders representing orientations comprising more particles. **e** Local resolution presented as coloring of the TRPV6_{THCV} cryo-EM map.



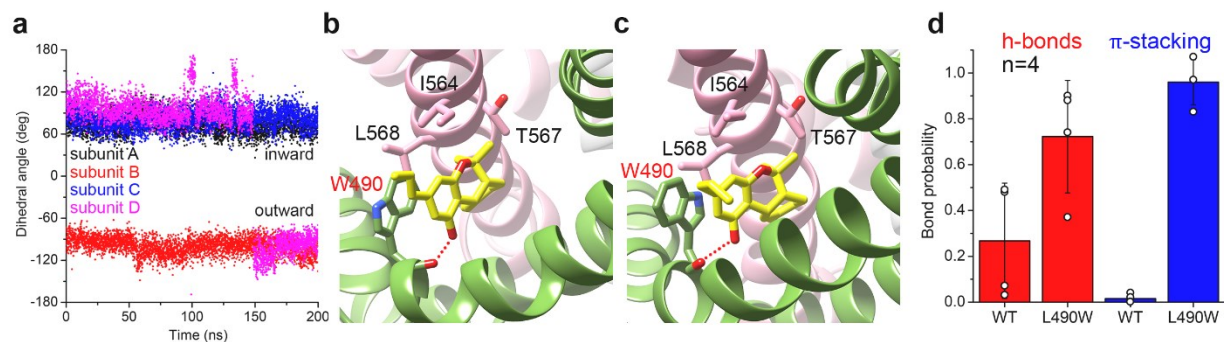
Supplementary Fig. 3 | Maps and LigPlot analysis for THCV binding. a–d Maps for THCV (red mesh) and surrounding protein (blue mesh). Shown are the final map at different contour levels (**a,b**) as well as half maps A (**c**) and B (**d**). **e,f** LigPlot analysis for THCV sites 1 (**e**) and 2 (**f**).



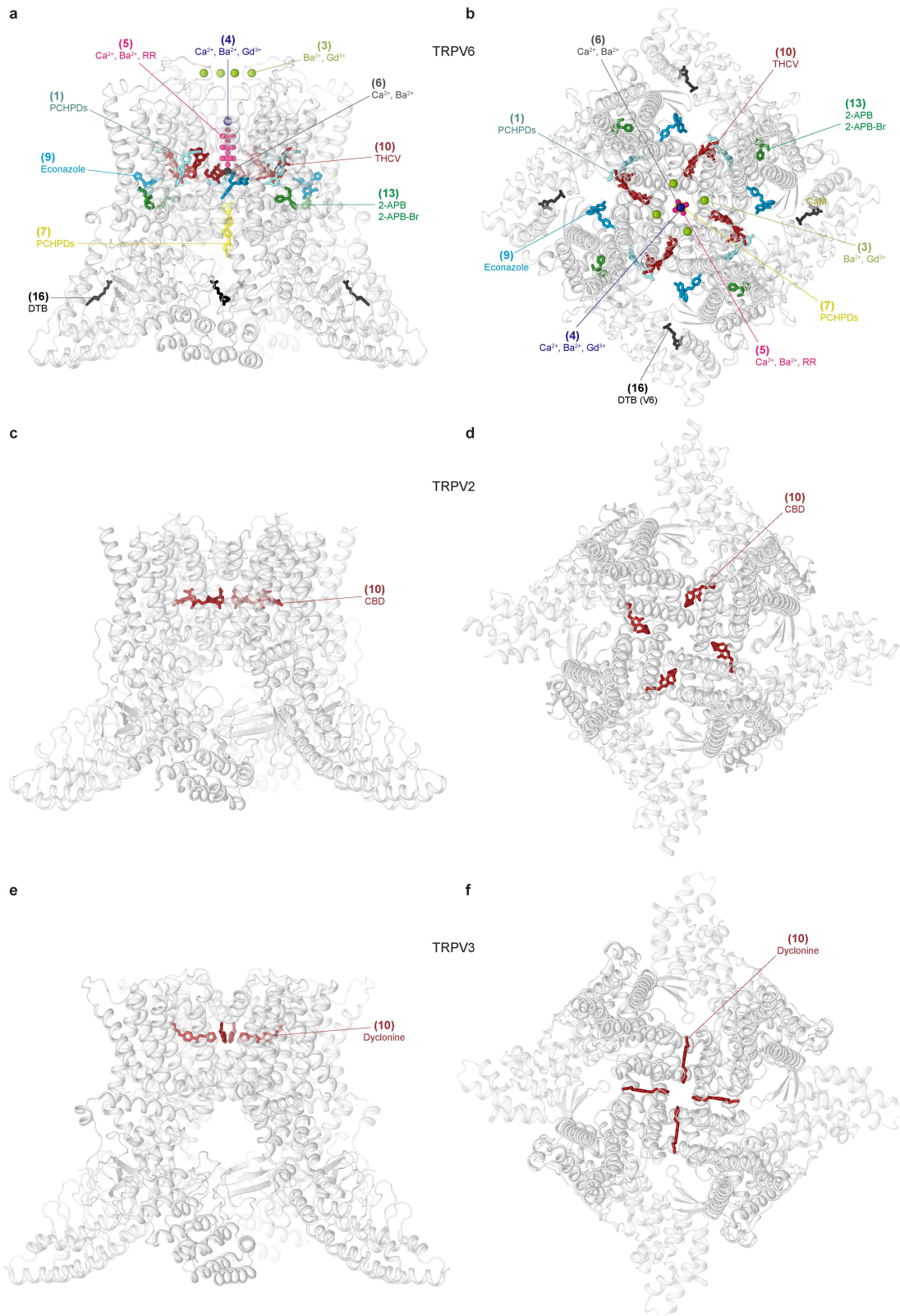
Supplementary Fig. 4 | FSEC and functional characterization of hTRPV6 mutants. **a–h** FSEC profiles for wild type (**a**) and mutant (**b–h**) hTRPV6. Note the major tetrameric peak eluting at ~25 min. **i–l** Whole-cell patch-clamp currents recorded from HEK 293 cells expressing wild type (**i**) or mutant (**j–l**) hTRPV6 in response to -100 to 70 mV voltage ramp. Examples are representatives of currents recorded from 3 to 20 different cells in two to four independent transfections. **m** Concentration-dependencies of Ca^{2+} uptake activation by calcium fitted with the logistic equation (curves through the points), with the EC_{50} values of 1.05 ± 0.03 mM ($n = 3$) for wild type hTRPV6, 1.33 ± 0.04 mM ($n = 3$) for L490W, 1.05 ± 0.12 mM ($n = 3$) for M497A, 0.39 ± 0.02 mM ($n = 3$) for A561W, and 0.50 ± 0.02 mM ($n = 3$) for I564A. Data points are mean \pm SEM. Source data are provided as a Source Data file. **n** Concentration-dependencies of 10 mM Ca^{2+} -induced Ca^{2+} uptake inhibition by econazole fitted with the logistic equation (curves through the points), with the IC_{50} values of 4.73 ± 0.13 μM ($n = 9$) for wild type hTRPV6, 10.7 ± 0.7 μM ($n = 3$) for L490W, 4.29 ± 0.58 μM ($n = 3$) for M497A, 6.55 ± 0.34 μM ($n = 3$) for A561W, and 4.26 ± 0.26 μM ($n = 3$) for I564A. Data points are mean \pm SEM. Source data are provided as a Source Data file. **o** Representative ratiometric Fura-2-based fluorescence measurements of changes in intracellular Ca^{2+} for HEK 293S GnTI $^{-}$ cells expressing L490W mutant hTRPV6 channels. The changes in the fluorescence intensity ratio at 340 and 380 nm (F_{340}/F_{380}) were monitored in response to application of 10 mM Ca^{2+} (arrow) after pre-incubation of cells without and with 100 μM of ion channel blocker Gd^{3+} . The experiment was repeated independently three times with similar results.



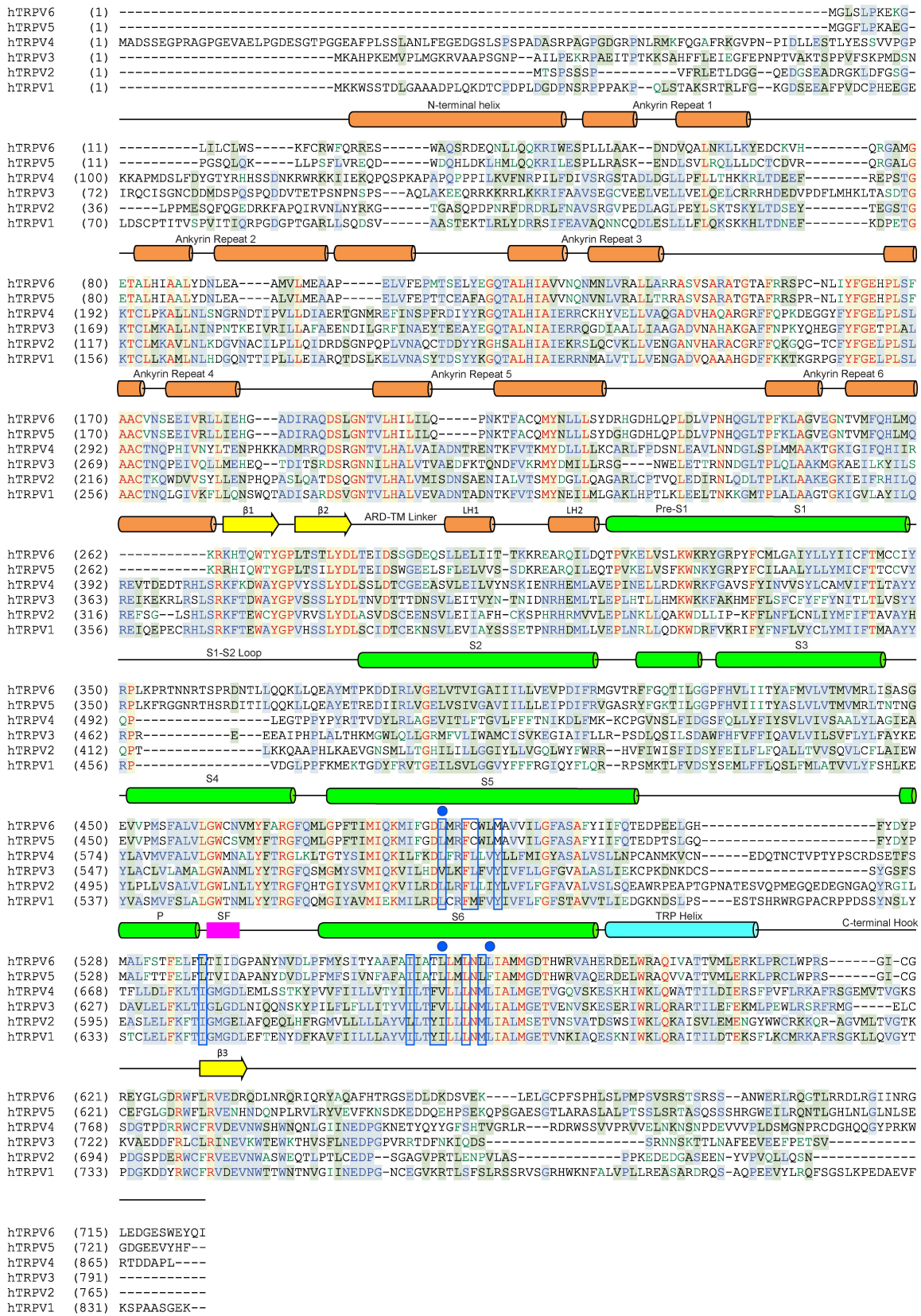
Supplementary Fig. 5 | Additional details of MD simulation of THCv binding to TRPV6. **a** THCv leaving site1 of the open TRPV6 along the horizontal pathway. Yellow, orange, and red sticks show three successive MD-snapshots of THCv along the leaving path. Cryo-EM model of protein is shown as green (subunit A) and pink (subunit B) cartoon. Hydrogen bonds between THCv-L490 and T581-D489 are shown as red dotted lines. **b** THCv vertical pathway is shown as a black curve, with energy minima along the pathway indicated by red segments M1, M2 and M3. Surface of subunit A, subunit B and F534 is colored green, pink and blue, respectively. Molecules of CHS (white) and THCv (yellow) at site 1 are shown as sticks. **c** Potential of mean force calculated along the vertical pathway, with the energy minima M1, M2, and M3 highlighted in pink. Blue, pink, and green lines indicate hydrogen bonds between THCv and L490, between THCv and other residues, and π -stacking interaction between THCv and F534, respectively. **d** THCv molecule with atoms colored according to the molecular hydrophobicity potential (MHP) on their surface, where hydrophobic and hydrophilic surfaces are shown in brown and blue, respectively. **e** Closeup view of THCv binding pocket, with protein surface colored according to the MHP. Molecules of THCv (yellow) and CHS (white) are shown in sticks.



Supplementary Fig. 6 | MD simulation of THCV binding to the TRPV6-L490W mutant. **a** Orientations of side chains of residues W490 during MD simulations. Dihedral angles for residues in four TRPV6 subunits are shown with different colors. The inward and outward orientations of W490 correspond to the dihedral angle (C_{α} - C_{β} - C_{γ} - $C_{\delta 2}$) values of 80° and -110° , respectively. **b,c** Close-up views of site 1 in the L490W mutant, with the tryptophan side chain in inward (**b**) and outward (**c**) orientations. **d** Average probability of hydrogen bond formation between THCV and residue 490 (red) and average probability of π -stacking interaction between THCV and aromatic residues in MD simulations of the wild-type and mutant channels. Data in **d** are mean over four independent THCV molecules, errors are \pm SD.



Supplementary Fig. 7 | THCv versus other TRPV6 ligands and portal site ligands in vanilloid-subfamily TRP channels. **a,b** Side (**a**) and top (**b**) views of hTRPV6_{THCV} (grey cartoon) with different TRPV6 binding sites mapped by differently colored ligands and numbered as described¹. The ligands include Ca^{2+} , Ba^{2+} and Gd^{3+} ions^{2,3}, desthiobiotin (DTB)², 2-aminoethoxydiphenyl borate (2-APB) and its brominated analog 2-APB-Br⁴, (4-phenylcyclohexyl)piperazine derivatives (PCHPDs)⁵, ruthenium red (RR)⁶, and econazole⁶. **c-d** Side (**c**) and top (**d**) views of rat TRPV2 (PDB ID: 6U88)⁷ with bound cannabidiol (CBD) molecule at the portal site shown in brown. **e,f** Side (**e**) and top (**f**) views of mouse TRPV3 (PDB ID: 7UGG) with bound dyclonine molecule at the portal site shown in brown.



Supplementary Fig. 8 | Sequence alignment of human vanilloid-subfamily TRP channels. Secondary structure elements are depicted above the sequence as cylinders (α -helices), arrows (β -strands), and lines (loops). The pink rectangle marks the selectivity filter. Blue boxes indicate residues involved in THC binding to site 1. Mutated residues are labeled with blue circles.

Supplementary Table 1 | Cryo-EM data collection, refinement and validation statistics

| | |
|---|------------------------|
| Structure | hTRPV6 _{THCV} |
| EMDB accession code | EMD-40676 |
| PDB accession code | 8SP8 |
| Data collection and processing | |
| Magnification | 130,000x |
| Voltage (kV) | 300 |
| Electron exposure (e ⁻ Å ⁻²) | 60 |
| Defocus range (µm) | -0.8 to -2.0 |
| Reported pixel size (Å) | 0.825 |
| Exposures (no.) | 6,699 |
| Processing software | |
| Motion correction | cryoSPARC v3.3 |
| CTF estimation | cryoSPARC v3.3 |
| Platform software for particle picking | cryoSPARC v3.3 |
| Software for 2D/3D class. & Refinements | cryoSPARC v3.3 |
| Symmetry imposed | C4 |
| Initial particle images (no.) | 4,502,785 |
| Final particle images (no.) | 213,249 |
| Map resolution (Å) | 2.79 |
| FSC 0.143 | |
| Refinement | |
| Initial models used (PDB code) | 7S8C |
| Model resolution (Å) | 2.79 |
| FSC threshold | 0.143 |
| Map sharpening <i>B</i> factor (Å ²) | -111.0 |
| Model composition | |
| Non-hydrogen atoms | 21,082 |
| Protein residues | 2,456 |
| Ligands | 42 |
| <i>B</i> factors (Å²) | |
| Protein | 92.79 |
| Ligands | 33.66 |
| R.m.s. deviations | |
| Bond lengths (Å) | 0.010 |
| Bond angles (°) | 1.066 |
| Validation | |
| MolProbity score | 1.55 |
| Clash score, all atoms | 1.93 |
| Poor rotamers (%) | 0.00 |
| Ramachandran plot | |
| Favored (%) | 91.80 |
| Allowed (%) | 8.20 |
| Disallowed (%) | 0.00 |

Supplementary Table 2 | List of MD runs

| Run name | Simulation duration | Ligand starting position | Description |
|-------------|---------------------|--------------------------------|--|
| fwd_run1 | 40+200 ns* | pose 1 (like in cryo-EM model) | Forward orientation of THCV molecules in sites 1 of TRPV6 _{THCV} . |
| fwd_run2 | 40+50 ns* | pose 2 | |
| fwd_run3 | 40+50 ns* | pose 3 | |
| fwd_run4 | 40+50 ns* | pose 4 | |
| bwd_run1 | 40+50 ns* | pose 5 | Backward orientation of THCV molecules in sites 1 of TRPV6 _{THCV} . |
| bwd_run2 | 40+50 ns* | pose 6 | |
| bwd_run3 | 40+50 ns* | pose 7 | |
| bwd_run4 | 40+50 ns* | pose 8 | |
| open_run | 40+50 ns* | pose 1 (like in cryo-EM model) | Forward orientation of THCV molecules in sites 1 of open TRPV6 (PDB ID 7S88). |
| L490W_run | 40+200 ns* | pose 1 (like in cryo-EM model) | Forward orientation of THCV molecules in sites 1 of L490W mutant of TRPV6 _{THCV} . |
| pulling_run | 50 ns | pose 1 (like in cryo-EM model) | Pulling of THCVs from sites 1 of TRPV6 _{THCV} . |
| umb_runs | 32 × 5 ns | poses from pulling_run | 32 starting configurations for umbrella sampling windows, two THCV molecules were chosen for the umbrella simulation: lig2 (vertical pathway) and lig4 (horizontal pathway). |

* 40 ns of equilibration were included in the analyzed data set.

Supplementary References

- 1 Yelshanskaya, M. V. & Sobolevsky, A. I. Ligand-Binding Sites in Vanilloid-Subtype TRP Channels. *Front Pharmacol* **13**, 900623, doi:10.3389/fphar.2022.900623 (2022).
- 2 Saotome, K., Singh, A. K., Yelshanskaya, M. V. & Sobolevsky, A. I. Crystal structure of the epithelial calcium channel TRPV6. *Nature* **534**, 506-511, doi:10.1038/nature17975 nature17975 [pii] (2016).
- 3 Singh, A. K., Saotome, K. & Sobolevsky, A. I. Swapping of transmembrane domains in the epithelial calcium channel TRPV6. *Sci Rep* **7**, 10669, doi:10.1038/s41598-017-10993-9 (2017).
- 4 Singh, A. K., Saotome, K., McGoldrick, L. L. & Sobolevsky, A. I. Structural bases of TRP channel TRPV6 allosteric modulation by 2-APB. *Nat Commun* **9**, 2465, doi:10.1038/s41467-018-04828-y (2018).
- 5 Bhardwaj, R. *et al.* Inactivation-mimicking block of the epithelial calcium channel TRPV6. *Sci Adv* **6**, eabe1508, doi:10.1126/sciadv.abe1508 (2020).
- 6 Neuberger, A., Nadezhdin, K. D. & Sobolevsky, A. I. Structural mechanisms of TRPV6 inhibition by ruthenium red and econazole. *Nat Commun* **12**, 6284, doi:10.1038/s41467-021-26608-x (2021).
- 7 Pumroy, R. A. *et al.* Molecular mechanism of TRPV2 channel modulation by cannabidiol. *Elife* **8**, e48792, doi:10.7554/eLife.48792 (2019).